Targeting NRP1 with EG00229 induces neurovascular permeability

Silvia Dragoni[1$], James T. Brash[1], Alessandro Fantin[1,2], Charles Burridge[1,3], Laura Denti[1,4], Patric Turowski[1] and Christiana Ruhrberg[1,$]

[1] University College London, 11-43 Bath Street, London EC1V 9EL, UK
[2] current affiliation: Department of Biosciences, University of Milan, Via G. Celoria 26, 20133 Milan, Italy
[3] current affiliation: Department of Chemistry and Molecular Biology, University of Gothenburg, 405 30, Göteborg, Sweden
[4] current affiliation: Francis Crick Institute, 1 Midland Rd, London NW1 1AT, UK

[$] corresponding authors: Dr Silvia Dragoni; s.dragoni@ucl.ac.uk
Professor Christiana Ruhrberg; c.ruhrberg@ucl.ac.uk

ORCID IDs:
Silvia Dragoni 0000-0002-9107-6291
James Brash 0000-0003-0420-031X
Alessandro Fantin 0000-0002-5517- 6068.
Charles Burridge 0000-0002-6321-4052
Laura Denti 0000-0002-6000-5765
Christiana Ruhrberg 0000-0002-3212-9381
Patric Turowski 0000-0002-7660-5802

Keywords: vascular permeability, endothelial cell, retina, EG00229, VEGF, NRP1, KDR, FLT1

Statements and Declarations. The authors have no competing interests to declare.

Contributions. SD, AF, JTB, PT and CR conceived and designed the study. SD performed most of the experiments. JTB, AF and PT performed some of the experiments. CB prepared the schematic representation of the crystal structures and corresponding interaction diagrams. SD and AF analysed data. LD bred and genotyped mice. SD and CR co-wrote the manuscript. All authors have read, commented on and approved the submitted manuscript.

Acknowledgements. We thank the Biological Resources team and Yaiza Yuste Herranz for technical help. This study was supported by research grants from the Wellcome Trust (095623/Z/11/Z), British Heart Foundation (PG/14/81/31119, PG/17/70/33232) and MRC (MR/N011511/1) to CR, British Heart Foundation (FS/13/59/30649) to JTB, Diabetes UK (Ref 17/0005637) to PT and SD and a Moorfields Eye Charity Career Development Award (GR001458) to SD.

Abstract

NRP1 is a therapeutic target for inhibiting vascular endothelial growth factor (VEGF)-induced blood vessel dysfunction. The small molecule EG00229 was designed to inhibit VEGF binding to NRP1 and reduce pathological blood vessel growth. However, it is unknown whether EG00229 could also be used to reduce VEGF164-induced vascular leakage, which often exacerbates ischemic diseases due to VEGF upregulation. Here, we show that prior treatment with EG00229 prevents VEGF164-induced vascular permeability signalling, but, unexpectedly, also find that EG00229 increased rather than inhibited vascular leakage. Thus, EG00229 increased vascular leakage either when added alone or concurrently with VEGF164, both in perfused retinal explants and across primary brain EC monolayers. This EG00229-induced vascular leakage was not an off-target effect, because it relied on endothelial NRP1 expression and NRP1's VEGF164 binding pocket, yet was independent of VEGFR1 and VEGFR2. Moreover, EG00229 activated molecular events typical of VEGF164-induced paracellular permeability, including p38 MAP kinase (p38) and SRC family kinase (SFK) phosphorylation as well as CDH5 rearrangement in endothelial junctions. Investigating EG00229-induced signalling therefore helps elucidate NRP1-dependent mechanisms of paracellular permeability induction and might help identifying new approaches to modulate the neurovascular barrier.

Introduction

Neuropilin 1 (NRP1) acts in several cell types as a coreceptor for the VEGF165 isoform of the vascular endothelial growth factor A (VEGF) or SEMA3 proteins to variably promote normal neuronal patterning, blood vessel growth or vascular remodelling [1,2]. NRP1 also binds VEGF165 and SEMA3 proteins to drive pathological processes, for example, neovascularisation, vascular permeability, immune cell activation, tumour cell migration and metastasis [3,4,2,5-7]. Accordingly, NRP1 is a target for therapeutic developments seeking to modulate NRP1-driven processes such as vascular dysfunction, cancer progression or defective nervous system repair [4,6,7]. Thus, antibodies have been developed to target NRP1's a1a2 versus b1 domains to selectively impair SEMA3 or VEGF165 binding to NRP1 [8,9]. Most strategies pursuing NRP1 inhibition have, however, homed in on NRP1's binding pocket for C-end rule (CendR) peptides, whose carboxyl-terminal arginine (R)-x-x-R motif docks to a binding pocket in the NRP1 b1 domain [10]. A CendR motif is constitutively found at VEGF165's C-terminus and is exposed at SEMA3A's C-terminus after furin cleavage [11,12]. Furin cleavage can also expose a CendR motif in the S1 subunit of SARS-CoV-2's spike protein, and S1 docking to NRP1 enhances viral internalisation after ACE receptor binding on target cells [13,14].

CendR-based NRP1 inhibitors include several peptides, peptidomimetics and small molecule antagonists [15-17,14,18]. When constructing peptide and peptidomimetic antagonists, the C-terminal arginine is retained for interaction with aspartate 320 (D320) in the CendR binding pocket, and in small-molecule antagonists is typically substituted by arginyl moieties that engage D320. The synthetic peptide RPARPAR also binds NRP1's CendR pocket [11]. However, rather than acting as an inhibitor, multivalent RPARPAR, immobilised on particles, induces NRP1-mediated internalisation of payloads into cells and tissues, such as drugs to target NRP1-expressing tumour cells [11]. Moreover, multivalent RPARPAR peptides can increase vascular leakage in the Miles assay of vascular permeability and disrupt the barrier of primary human ECs (HUVEC) via NRP1's cytoplasmic domain (NCD) in an otherwise elusive mechanism [12].

EG00229 is a small molecule that inhibits VEGF-induced, NRP1-dependent endothelial and tumour cell migration by binding NRP1's CendR pocket [18] and has served as a prototype for other NRP1 inhibitors [17]. Prior work demonstrated that EG00229 has anti-tumoral activity. For example, EG00229 suppresses NRP1-mediated nasopharyngeal carcinoma cell migration and invasion [19]. Moreover, EG00229 increases the potency of the cytotoxic agents paclitaxel and 5-fluorouracil in lung adenocarcinoma cells [18] and synergises with lenvatinib to inhibit cholangiocarcinoma cells, which rely on NRP1 to grow and metastasise [20]. EG00229 also enhances the anti-tumour activity of microglia in a mouse glioma model [21]. With multiple roles in blocking tumour cells as well as tumour angiogenesis, EG00229 is considered useful for NRP1 blockade in cancer therapy [19]. More recently, EG00229 was reported to impair NRP1 binding of the SARS-CoV-2 S1 spike protein, which carries a CendR motif, to Caco-2 cells, thereby suggesting that NRP1 inhibition might be useful to

treat COVID-19 [14]. Further, EG00229 and S1 can both compete with VEGF165 for NRP1-induced sensory neuron firing to modulate pain perception [22].

Although NRP1 inhibition has also been proposed as a therapeutic strategy to complement current anti-VEGF approaches to treat neovascular eye diseases [23-25], it has not been examined whether a CendR-based NRP1 inhibitor such as EG00229 would be suitable to reduce VEGF-induced vascular leakage from retinal vasculature. Here, we have investigated how EG00229 affects the barrier function of retinal and brain (neurovascular) endothelial cells and unexpectedly found that it increased acute vascular leakage and permeability signalling.

Methods

Structural models. The published crystal structures for VEGF165 in complex with NRP1 (PDB:4deq) [33] and EG00229 (chain B, PDB:3i97)[18] were rendered with PyMOL Molecular Graphics System 1.0 v2.5.0 (Schroedinger LLC) [34] and the academic version of Ligplot+ v2.2 was used to produce molecular interaction diagrams [35].

Animals. Animal work was performed following UK Home Office Animals in Science Procedures e-Licensing (ASpeL) and institutional Animal Welfare and Ethical Review Body (AWERB) guidelines. To produce mice with an endothelial-specific NRP1, VEGFR1 (FLT1) or VEGFR2 (KDR) deletion, we combined *Cdh5*-CreER^{T2} with floxed conditional null alleles *Nrp1* (*Nrp1*$^{fl/fl}$) [26], *Kdr* (*Kdr*$^{fl/fl}$)[27] and *Flt1* (*Flt1*$^{fl/fl}$) [28]. To induce gene deletion, sex-matched Cre-positive and Cre-negative young adult littermates were each injected with 0.5 mg tamoxifen (Sigma-Aldrich) in 250 µl peanut oil (Sigma) once a week for 2 weeks; the last tamoxifen injection was performed 6 days before permeability-relevant experiments. We also used NCD-deficient mice (*Nrp1*$^{cyto/cyto}$) and mice with a CendR pocket mutation (*Nrp1*$^{D320K/D320K}$) together with wild type littermate controls [29,30]. All mice were maintained on a C57Bl/6J background (The Jackson Laboratory). We used both male and female mice in this study, with no obvious difference in the data obtained for both sexes.

***Ex vivo* retina permeability assay.** Retinal explants were prepared as described [31]. Briefly, adult mice were culled by CO_2 overdose and the common carotid artery was cannulated to perfuse the vasculature with heparinised saline followed by cardioplegic solution (10 mM Mg^{2+}, 110 mM NaCl, 8 mM KCl, 10 mM HEPES and 1 mM $CaCl_2$, pH 7.0) containing 10 µM isoproterenol, and finally with cardioplegic solution supplemented with 5 g/l Evans Blue dye and 10% bovine serum albumin (BSA) w/v (5 ml of each solution per mouse). From each mouse, both eyes were surgically removed for further microdissection. One retina was used for immunostaining (see below) and the other retina, together with the attached sclera, was flattened onto a transparent silicone base (SYLGARD 184, Merck) and maintained in position with a metal ring. These retinal explants were mounted on an

130 upright Axiophot fluorescence microscope (Zeiss) and continuously superfused with Krebs solution
131 (124 mM NaCl, 5 mM KCl, 2 mM $MgSO_4$, 0.125 mM NaH_2PO_4, 22 mM $NaHCO_3$ and 2 mM $CaCl_2$,
132 pH 7.4) containing 5 mM glucose and 0.1% BSA w/v. A radial vessel was cannulated using a glass
133 needle, through which the retinal vasculature was injected with 1 mg/ml sulforhodamine B (479 Da;
134 Merck) in Krebs solution. For permeability measurements, the fluorescent content of a microvessel
135 was recorded continuously by time-lapse imaging using a CCD camera (Hamamatsu) and
136 HCImageLive software (Hamamatsu) for at least 2 min. Specifically, the baseline sulforhodamine B
137 signal was recorded for ~30 s before VEGF164 or EG00229 were added dropwise onto the retina.
138 Recording continued for at least 90 s. Time-lapse series were analysed using ImageJ (NIH
139 Bethesda). Pixel intensity measurements were plotted against time, and permeability values were
140 computed by fitting data to the exponential equation $Ct = C0 \times e^{-kt}$, whereby $k = 4\ P/d$ and d is the
141 diameter of the vessel [32]. The difference in signal intensity of the fluorescent content of a
142 microvessel between pre-treatment and post-treatment reflected the absolute permeability change
143 due to treatment. Permeability measurements from at least three different *ex vivo* retinal preparations
144 were combined and expressed as mean ± SD. Statistical analysis included a repeated measures
145 two-way ANOVA to compare the baseline, VEGF164-induced and EG00229-induced vascular
146 permeability in the control versus mutant retina or with and without pharmacological inhibitors in wild
147 type retina.
148
149 **Retinal immunostaining.** Mouse retinae were fixed in 4% formaldehyde in PBS for 1h and
150 wholemount immunostained as described [31] using rabbit anti-P-p38 MAPK (Thr180/Tyr182)
151 antibody (Cell Signaling) followed by Alexa Fluor 555–conjugated goat anti–rabbit antibodies
152 (Invitrogen) and biotin-conjugated IB4 (Merck) followed by Alexa Fluor 488-conjugated streptavidin
153 (Invitrogen). Images were acquired with Zeiss Axioskop 2 microscope, using a ph3 Plan-Apochromat
154 63x/1.40 oil objective, Hamamatsu camera and the HCImage software. Images were processed with
155 ImageJ software version 1.52a (NIH Bethesda). Each image was acquired as an RGB colour image.
156 Channels were split to separate the IB4 staining (green channel) from the P-p38 staining (red
157 channel). The threshold function was used on the IB4 image to create a mask of the vascular area
158 that was transferred onto the P-p38 image to identify vascular P-p38 staining; the P-p38 area was
159 normalised against the IB4 area. Two-way ANOVA was used to compare genotypes and treatments.
160
161 **Pharmacological inhibitors.** The NRP1 inhibitor EG00229, the VEGFR2 inhibitor SU1498, the P38
162 inhibitor SB203580 and the SFK inhibitor PP2 were all purchased from MERCK (Dorset, United
163 Kingdom) and used at a concentration of 10 μM unless otherwise specified.
164
165 **Primary rat brain EC isolation, transendothelial flux assay and immunostaining.** Microvessels
166 from adult male or female rat brains were isolated by collagenase/dispase digestion and BSA/Percoll
167 density gradient centrifugation as described [32]. Purified vessels were seeded onto 12 mm

168 transwells (Costar) coated with collagen IV and fibronectin (Merck) and cultured in EGM2-MV media
169 (Lonza). Media were supplemented with 5 µg/ml puromycin for the first 5 days after plating. Cells
170 were cultured for 2–3 weeks in total until their trans-endothelial electrical resistance (TEER)
171 plateaued at values above 200 Ω cm^2. The TEER was measured using STX-2 chopstick electrodes
172 connected to an EVOM voltohmmeter (World Precision Instruments). 1 mg/ml 4 kDa fluorescein
173 (FITC)-dextran was added to the apical ('luminal') side of the brain microvascular ECs grown on the
174 transwells before permeability measurements were performed as described [32]. Briefly, 50 µl
175 samples of medium were removed from the basal chamber and replaced with fresh medium at 20
176 min intervals for 120 min before and after adding 50 ng/ml VEGF164 or 10 µM EG00229 to the apical
177 or basal side of the transwell cultures. Sample fluorescence was measured with a microplate reader
178 (Tecan Safire) and readings plotted against time. Fluorescence changes along the linear slope
179 before and after adding an agent provided a measure of vascular permeability induction [32]. Linear
180 slope changes of three different wells from the same cell preparation were averaged and the average
181 considered as n = 1. Data are means ± SD of at least three independent preparations. Statistical
182 analysis included unpaired Student's t-test followed by a post-hoc Dunn's test, with a significance
183 level set at 0.05. In some experiments, primary rat brain ECs cultured on transwells were fixed in
184 4% formaldehyde in PBS for 15 minutes, permeabilised with acetone (-20°C) and left in blocking
185 buffer (PBS 0.5% BSA) for 5 minutes. Cells were then immunostained using CDH5 antibody [36]
186 diluted 1:100 in blocking buffer for 30 min followed by Alexa Fluor 555–conjugated goat anti–rabbit
187 antibodies (ThermoFisher) diluted 1:200 in blocking buffer together with Hoechst. Images were
188 acquired with a Zeiss Axioskop 2 microscope, using a ph3 Plan-Apochromat 63x/1.40 oil objective,
189 Orca ER camera (Hamamatsu) and HCImage software (Hamamatsu). Images were processed with
190 ImageJ software version 1.52a (NIH Bethesda).
191
192 **Human brain ECs.** Cells from the human brain microvascular EC line hCMEC/D3 [37] were seeded
193 on collagen I-coated 35 mm tissue culture dishes (Nunc) and grown in EGM2-MV (Lonza).
194
195 **Immunoblotting.** Cell lysates from primary rat ECs or hCMEC/D3 were prepared as described [31].
196 Lung tissue from tamoxifen-treated mice and their littermate controls was homogenized and lysed in
197 RIPA buffer, in the presence of 0.1% SDS, protease inhibitor cocktail 2 and phosphatase inhibitor
198 cocktail (Sigma-Aldrich). Proteins were separated by SDS-PAGE and transferred to nitrocellulose
199 by semi-dry electrotransfer. Membranes were blocked overnight and then incubated with the
200 appropriate primary antibody diluted in TBS containing 0.1% Tween-20, 1% bovine serum albumin
201 (BSA) for 2 h at room temperature; the primary antibodies used were specific for P38 (MAPK14),
202 SRC, VEGFR2, VEGFR1 or NRP1, and for the activated (phosphorylated) forms of P38 or SRC
203 family kinases (SFK) (1:1000; all from Cell Signaling Technology), and GADPH or tubulin (1:10000;
204 Merck). Membranes were washed twice with TBS containing 0.1% Tween-20 and once with PBS
205 containing 0.1% Tween-20 and then incubated with goat anti-mouse or goat anti-rabbit horseradish

206 peroxidase (HRP)-conjugated IgG (GE Healthcare) diluted 1:10000 or 1:5000, respectively, in PBS
207 containing 0.1% Tween-20, 1% BSA. Membranes were developed using the ECL reagents (Roche)
208 with the Bio-Rad ChemiDoc MP Imaging System and images were acquired using the Bio-Rad
209 Image Lab software (version 6.0.1). Protein bands were evaluated by densitometric quantification,
210 whereby signal intensity was normalised to signal intensity from GADPH or tubulin from the same
211 sample as a loading control. Phosphorylation levels of P38 and SKHs were normalised against the
212 total levels of P38 or SRC. Densitometric quantification of three independent immunoblots were
213 determined by changes in protein or phosphoprotein content normalised to tubulin or GADPH total
214 protein loading controls, with values expressed as fold increase. Data are shown as mean ± SD.
215 Statistical analysis included one-way ANOVA followed by post-hoc Dunnett's tests.
216

217 **Results**

218 **EG00229 induces retinal vascular leakage**

219 To determine whether EG00229 functions as a competitive inhibitor in VEGF-induced vascular
220 leakage, we used an *ex vivo* assay of mouse retina that measures the extravasation of fluorescent
221 sulforhodamine B dye from perfused microvasculature [31], which can be recorded in real-time (**Fig.**
222 **S1A**). As shown [31], 10 ng/ml VEGF164 (mouse equivalent of human VEGF165) rapidly induced
223 dye extravasation from the retinal microvessel lumen, corresponding to a ~3-fold increase in
224 microvessel permeability (**Fig. 1A,B**). Consistent with analogous findings on VEGF inhibition in other
225 contexts, pre-incubating retinal explants for 15 min with 10 μM EG00229 significantly reduced
226 VEGF164-induced dye extravasation (EG00229→VEGF164; **Fig. 1A,B**). Unexpectedly, however,
227 adding 10 μM EG00229 alone also induced dye extravasation at a similar extent as VEGF164, and
228 adding EG00229 and VEGF164 together increased extravasation more than adding VEGF164 alone
229 (**Fig. 1A,B**). These findings show that EG00229, albeit able to inhibit VEGF164-dependent vascular
230 permeability, can also activate it independently of VEGF164. Therefore, we characterised the
231 EG00229 response in more detail. Re-treatment with VEGF164 and EG00229 after 15 min washout
232 induced dye extravasation again without altering efficacy, even when VEGF164 and EG00229
233 treatment was alternated (**Fig. S1C**). These findings suggest that both VEGF164 and EG00229 can
234 increase retinal vascular permeability transiently and reversibly. Although several studies have used
235 EG00229 at 10 μM [19-21], others have used 30 μM [22], 100 μM [18,13] or 2 μM [20]. We have
236 routinely used 10 μM EG00229, but EG00229 also induced retinal vascular leakage at 10-fold lower
237 or 10-fold higher concentrations (**Fig. 1C**). As leakage appeared maximal at 10 μM (**Fig. 1C**), this
238 dose was used in subsequent experiments. Together, these findings suggest that EG00229 is a
239 CendR mimetic that prevents VEGF-induced vascular permeability in retinal microvasculature, but
240 also increased it on its own, similar to VEGF164.
241

242 **EG00229 induced retinal vascular leakage through NRP1 but not VEGFR2 or VEGFR1**

Prior studies showed that NRP1 promotes VEGF164-induced vascular permeability in the dermis together with VEGFR2 [30]. We, therefore, examined whether EG00229 also induced vascular leakage in the retina of mice after endothelial knockdown of VEGFR2, which is encoded by *Kdr*. This, we administered tamoxifen to adult *Kdr*$^{fl/fl}$ mice expressing or lacking *Cdh5*-CreER^{T2} [30]. In these experiments, knockdown in adulthood, after completion of vascular development, ensured normal retinal vascular density. Immunoblotting confirmed VEGFR2 knockdown (**Fig. 2A**). Agreeing with pharmacological VEGFR2 inhibition [31], VEGF164-induced dye extravasation in retinal explants was abolished by VEGFR2 knockdown, whereas EG00229-induced dye extravasation was not (**Fig. 2B**). As VEGFR1 interacts with NRP1 in vitro [38] and promotes VEGF signalling together with NRP1 during psoriasis-like disease [39] and in snake venom-induced dermal vascular leakage [40], we next examined how endothelial VEGFR1 knock-down affected retinal vascular leakage by targeting the VEGFR1 gene, *Flt1*. Thus, we administered tamoxifen to adult *Flt1*$^{fl/fl}$ mice expressing or lacking *Cdh5*-CreER^{T2} and confirmed VEGFR1 knockdown (**Fig. 2C**), but found that it did not impair VEGF164- or EG00229-induced dye extravasation (**Fig. 2D**). By contrast, endothelial NRP1 knockdown significantly reduced both VEGF164- or EG00229-induced dye extravasation (**Fig. 2E,F**). Notably, NRP1 knockdown did not abrogate VEGF164-induced leakage completely (**Fig. 2F**), which agrees with prior findings in the dermis, where VEGFR2 is absolutely required but NRP1 enables a robust response [30]. Compared to VEGF164, dye extravasation induced by EG00229 was affected more severely by endothelial NRP1 knockdown (**Fig. 2F;** the reduction in extravasation in individual mice correlated with knockdown efficiency). This finding shows that NRP1 is required for EG00229-induced retinal vascular leakage, thereby demonstrating that this response is not an off-target effect.

EG00229 induced retinal vascular leakage via NRP1's CendR pocket but not the NCD

Next, we analysed *Nrp1*$^{D320K/D320K}$ mice in which the D320 residue in NRP1's CendR pocket is replaced with K [30,41]. These mice have normal NRP1 levels (**Fig. 2G**), but impaired VEGF164 binding to NRP1 [41]. In analogy to findings in the dermis [30], VEGF164-induced retinal vascular leakage was attenuated in *Nrp1*$^{D320K/D320K}$ mice (**Fig. 2H**). EG00229-induced retinal vascular leakage was also significantly reduced in these mice (**Fig. 2H**), again corroborating that this response is not an off-target effect but a NRP1-dependent, CendR pocket-mediated mechanism.

Prior work showed that NRP1's NCD synergises with NRP1's VEGF binding domain to promote complex formation between VEGFR2 and NRP1 to enhance VEGF164-induced VEGFR2 signalling [42,43]. In agreement, *Nrp1*$^{cyto/cyto}$ mice lacking the NCD have reduced VEGF164-induced vascular leakage in the dermis [30]. We confirmed that NRP1 protein in *Nrp1*$^{cyto/cyto}$ mice was stable despite lacking the NCD (**Fig. 2I**). Although VEGF164-induced dye extravasation was attenuated in *Nrp1*$^{cyto/cyto}$ mice, EG00229-induced dye extravasation was not (**Fig. 2J**). The finding that EG00229 did not require the NCD to induce vascular leakage thus distinguished its mechanism of action from that of VEGF164 and a multivalent RPARPAR peptide, which both require the NCD.

281

282 **VEGF165 and EG00229 bind similarly to NRP1's b1 domain**

283 To better understand why EG00229 has the capacity to signal via NRP1, similar to VEGF164,
284 we compared the published X-ray crystal structures of NRP1's b1 domain in complex with VEGF164
285 versus EG00229 [18,44,41,33]. Thus, we used PyMol and LigPLOT+ to compare VEGF164's exon
286 7-8 domain (PDB:4deq) versus EG00229 (PDB:3i97), which illustrated that both ligands interact in
287 a similar manner with NRP1's CendR pocket (**Fig. 3A,B**). Firstly, they form salt bridges with D320
288 via VEGF165's terminal arginine EG00229's arginyl moiety (**Fig. 3C,D**) and hydrogen bonds with
289 S346, T349 and Y353. VEGF165's exon 7 has additional interactions with NRP1's L1 loop via T299
290 and N300 (**Fig. 3C**), whose replacement with analogous residues from NRP2 reduces VEGF165
291 binding [33]. Secondly, EG00229 interacts with NRP1's L1 loop, similar to VEGF165, via a stacking
292 interaction between the benzothiadiazole ring and N300 [18] and forms a hydrogen bond with S298
293 that has not previously been commented on (**Fig. 3D**). Y297 appears to contribute to shaping the
294 binding pocket via nonpolar interactions with VEGF165 and EG00229 and an additional hydrogen
295 bond with VEGF165 that is absent with EG00229 (**Fig. 3C**). The striking similarity in NRP1's b1
296 interactions with VEGF165 and EG00229 raised the possibility that EG00229 binding to the CendR
297 pocket might activate similar NRP1-dependent signalling pathways as those known to mediate
298 VEGF164-induced vascular permeability.

299

300 **EG00229 induces retinal vascular permeability via SFK-induced p38 activation**

301 Next, we asked whether EG00229 induced endothelial signalling pathways implicated in retinal
302 vascular permeability. To begin, we examined T180/Y182 phosphorylation of p38 (encoded by
303 *Mapk14*), which is required for VEGF164-induced vascular leakage in the retina and brain [31,32].
304 Retinal wholemount immunostaining showed that EG00229 induced endothelial p38 T180/Y182
305 phosphorylation (P-p38), similar to VEGF164 (**Fig. 4A**). VEGFR2 knockdown attenuated VEGF164-
306 induced endothelial P-p38, but not EG00229-induced endothelial P-p38 in retinal vasculature (**Fig.
307 4A**), and VEGFR1 knockdown neither affected EG00229- nor VEGF164-induced endothelial P-p38
308 in retinal vasculature (**Fig. 4B**). NRP1 knockdown and the D320K mutation attenuated both
309 VEGF164- and EG00229-induced P-p38 in retinal vasculature (**Fig. 4C,D**). These results
310 demonstrate that EG00229 depends on NRP1 but not VEGFR1 or VEGFR2 for inducing a key
311 vascular permeability signalling pathway in the retina, and they corroborate our findings in the retinal
312 vascular leakage assay to show that the receptor requirement for VEGF164 and EG00229 differs
313 with respect to VEGFR2.

314 To further probe the signalling requirements for EG00229-induced endothelial signalling, we
315 used established small molecule inhibitors. First, we used SU1498 as an established inhibitor of
316 VEGF164-induced retinal vascular leakage [31] to determine whether a pharmacological approach
317 recapitulated our findings with EG00229 in genetic knockout mice. Agreeing with prior work, pre-
318 incubating the retina with SU1498 abolished sulforhodamine B extravasation induced by VEGF164

(**Fig. 5A**). By contrast, pre-incubating the retina with SU1498 did not diminish EG00229-induced dye extravasation (**Fig. 5A**). Therefore, a pharmacological approach corroborated that EG00229 does not require VEGFR2 to induce vascular leakage. Second, we used the p38 inhibitor SB203580, which decreases VEGF164-induced retinal vascular leakage [31]. SB203580 also significantly decreased EG00229-induced dye extravasation (**Fig. 5B**). Third, we used PP2 [46], which in dermal ECs disrupts VEGF164-induced permeability signalling [30]. Treatment with PP2 at 10 μM, which inhibits both SFK and p38 activation {Bain, 2003 #6076}, also effectively abolished EG00229-induced dye extravasation in the retina (**Fig. 5C**). Further, wholemount retinal immunostaining showed that EG00229-induced endothelial p38 activation was not impaired by SU1498 but SB203580 and PP2 (**Fig. 5D**).

Together, these findings demonstrate that p38 conveys EG00229-induced signals for retinal vascular leakage.

EG00229 induce paracellular permeability signalling in brain microvascular ECs

We next asked whether EG00229 also increased the permeability of brain vascular endothelium. For this experiment, we grew primary microvascular ECs isolated from rat brains on transwells without passaging, because this method preserves excellent junctional barrier properties for flux studies as a proxy of extravasation from microvessels [32].Thus, we measured fluorescent dextran flux across these brain endothelial monolayers (**Fig. S2A**). As shown [32,31], VEGF164 increased flux across the monolayer by nearly 2-fold (**Fig. S2B,C**). Similarly, EG00229 enhanced flux across the monolayer by nearly 2-fold (**Fig. S2B,C**).

To increase vascular leakage in brain ECs, VEGF164 activates p38 and SFK signalling [31,30,47]. Immunoblotting showed that EG00229 activates p38 in brain endothelial monolayers, which peaked around 5 min and returned to baseline 30 min after treatment (**Fig. 6A,B**). Further, immunoblotting with an antibody that detects tyrosine phosphorylation of the SFK catalytic domain (corresponding to Y419 in human SRC) showed that EG00229 also activates SFKs in brain endothelial monolayers with similar kinetics (**Fig. 6A**), and pre-incubating rat brain EC monolayers with PP2 significantly decreased EG000229-induced P-p38 (**Fig. 6C**). To investigate relevance for human brain EC, we used hCMEC/D3 cells, which are used to model the human blood-brain barrier [48,37]. Again, we found that EG00229 induced both p38 and SFK activation in these cells (**Fig. S2D**). The ability of EG00229 to induce vascular leakage signalling is therefore conserved from rodent to human brain ECs.

To increase vascular leakage, VEGF164 acts on intercellular junctions in a mechanism termed paracellular permeability, including in brain ECs [32]. This pathway involves VEGFR2-induced signal transduction events that likely modify the adherens junction component vascular endothelial (VE) cadherin (CDH5) by phosphorylation [49] and nitrosylation [50]; these modifications are reported to cause CDH5 redistribution in HUVEC cultures from a linear to a ‘zig-zag’ pattern [51], and in brain EC cultures from a linear pattern to focal broadening especially at tricellular junctions [31]. As

357 previously shown [31,52], CDH5 localised in such a broader pattern around contact sites in
358 VEGF164-treated compared to untreated rat brain EC monolayers (**Fig. 7A**). Similar overall CDH5
359 staining intensity before and after VEGF164 treatment agrees with CDH5 not being degraded after
360 VEGF164 treatment [49,50], but that modifications caused CDH5 redistribution [51]. A similar CDH5
361 redistribution, also without changes in staining intensity, occurred after EG00229 treatment of
362 monolayers (**Fig. 7B**). The broader CDH5 localisation after EG00229 treatment was particularly
363 obvious at tricellular junctions (**Fig. 7B**), as previously reported for VEGF164 treatment of brain EC
364 monolayers [31]. Together with the observed changes in SFK and p38 activation, CDH5 re-
365 distribution in brain ECs suggests that EG00229 increases paracellular permeability via pathways
366 that are similar to those induced by VEGF164, despite not needing VEGFR2 activation (**Fig. S3**).
367

368 **Discussion**

369 EG00229 was originally designed to inhibit VEGF164-induced NRP1 responses [18].
370 Accordingly, EG00229 pre-treatment inhibits VEGF164-binding to NRP1 with an IC_{50} of 8 μM in vitro
371 [18]. As NRP1 promotes vascular hyperpermeability in mouse models of ocular neovascular disease
372 [30,24], we asked whether EG00229 was effective in inhibiting VEGF164-induced retinal vascular
373 leakage. Indeed, 10 μM EG00229 attenuated VEGF164-induced sulforhodamine B leakage in the
374 *ex vivo* mouse retina model of vascular permeability (**Fig. 1**). However, adding EG00229 alone as a
375 control in our experiments also induced acute vascular leakage it (**Fig. 1**). Whereas EG00229's
376 ability to inhibit VEGF164 binding to NRP1 has been studied extensively, we are, to the best of our
377 knowledge, the first to identify that EG00229 can actively induce a biological response. Our findings,
378 therefore, suggest that testing EG00229 in the absence of another CendR ligand is an important
379 control when establishing its ability to inhibit NRP1-mediated responses. More broadly, our findings
380 suggest that drugs designed to bind NRP1's CendR pocket should be routinely screened for potential
381 effects on vascular permeability at neurovascular barriers.

382 Prior work showed that a multimerised CendR peptide (RPARPAR) and a NRP1 extracellular
383 domain-binding antibody induce vascular leakage via NRP1, independently of VEGFR2 [12,11]. To
384 explain VEGFR2 independence, it has been hypothesised that CendR peptide-induced NRP1
385 clustering stimulates NRP1 internalisation, because internalisation or vascular leakage were more
386 effectively induced by multivalent than monomeric RPARPAR peptide [11]. The small molecule
387 EG00229 lacks obvious molecular features present in multivalent agents that cluster NRP1, and,
388 therefore, it remains elusive how EG00229 binding to NRP1's CendR pocket induces vascular
389 leakage. To better understand VEGF165 versus EG00229 binding to NRP1, we directly compared
390 prior knowledge of their structural interactions with NRP1 (**Fig. 3**). Notably, the published X-ray
391 crystallography structures of VEGF165 versus EG00229 bound to NRP1 [18,33,41] showed similar
392 interactions between the ligands and NRP1's b1 domain (**Fig. 3**). Thus, the D320 requirement for
393 NRP1 binding has been demonstrated for VEGF165 [41,30] and, here, also for EG00229 (**Fig. 2**).
394 Also similar to VEGF1645, EG00229 interacts with N300 in NRP1's L1 loop [18,33] (**Fig. 3**). Similar

395 interactions with the L1 loop are not seen with other CendR-type ligands, such as tuftsin [53] and
396 the KDKPPR peptide [54]. Conceivably, therefore, EG00229 might differ from other CendR-like
397 NRP1 targeting compounds by being particularly adept at mimicking the VEGF165 C-terminus.
398 EG00229's dependence on NRP1 for leakage induction was confirmed in endothelial NRP1
399 knockout mice and in *Nrp1*$^{D320K/D320K}$ mice lacking a fully functional CendR pocket (**Fig. 2**). Whereas
400 endothelial NRP1 loss completely abolished leakage induction by EG00229, the D320K mutation did
401 not abolish it completely. Therefore, NRP1 is required to convey EG00229's effect, and the D320
402 residue is important for their interaction, confirming the specificity of EG00229's activity for NRP1.
403 Further mutation of other interacting residues may be required to completely disrupt the docking of
404 CendR ligands to NRP1's binding pocket.

405 To better define the molecular pathways through which EG00229 induced acute retinal
406 vascular leakage, we established EG00229's signalling requirements. Consistent with EG00229
407 lacking a VEGFR2 binding site, genetic or pharmacological VEGFR2 ablation did not affect
408 EG00229-induced sulforhodamine B extravasation from retinal vessels (**Fig. 2**). This finding is
409 reminiscent of those made for the aforementioned RPARPAR CendR peptide and a NRP1
410 extracellular domain-binding antibody that did not require VEGFR2 to induce leakage of dermal
411 vessels [12,11]. VEGFR2 independence of EG00229-induced retinal vascular leakage and p38
412 activation was not explained by a VEGFR1 role (**Figs. 2, 4**), even though VEGFR1 promotes dermal
413 vascular leakage in response to VEGF164 [40]. Taken together with prior results for the RPARPAR
414 peptide, it appears that VEGF receptor tyrosine receptor activation is not a general feature of NRP1's
415 CendR ligands but is important for VEGF164, which has both a CendR peptide domain and a VEGFR
416 binding domain.

417 We further show that the mechanisms of EG00229-induced retinal vascular leakage was
418 independent of NRP1's highly conserved intracellular domain, the NCD (**Fig. 2**) and therefore
419 differed from that of the multimerised CendR peptide RPARPAR and VEGF164, which both require
420 the NCD to induce vascular leakage [12][30]. In addition to providing knowledge of EG00229
421 signalling, our findings also contribute new knowledge of VEGF signalling. Thus, the receptor
422 requirement for VEGF164-induced vascular permeability responses in retinal permeability assays is
423 similar to that in dermal permeability assays with respect to VEGFR2 and NRP1, but different with
424 respect to VEGFR1, which contributes to VEGF164-induced dermal but not retinal vascular leakage.
425 Finding that VEGFR1 was not required for VEGF164-induced retinal vascular leakage agrees with
426 prior findings that VEGFR1 localises preferentially to the luminal side of brain and retina endothelium
427 (*35*), rather than the tissue-facing side of the endothelium that is exposed to VEGF both in vivo and
428 in our ex vivo assays.

429 To investigate whether EG00229 differs from RPARPAR or VEGF164 by differentially
430 activating downstream signal transducers, we have examined P38 and SFK phosphorylation. This
431 was important, because multimerised RPARPAR reportedly does not induce VEGFR2 or P38
432 activation and therefore differs from VEGF164 [12]. EG00229 activated p38, and inhibiting p38

activation with SB203580 attenuated EG00229-induced vascular leakage (**Fig. 5**). EG00229 therefore differed from multimerised RPARPAR [12], but acted similar to VEGF164 with respect to NRP1-dependent p38 activation [57,32,31,58], despite lacking obvious means of engaging VEGFR1 or VEGFR2 to activate downstream phosphorylation cascades. Next, we considered that VEGF-induced paracellular permeability signalling depends on VEGF164-induced SFK activation [59,45,60,47], which is NRP1-dependent [30]. Similar to VEGF164, EG00229 induced SFK activation (**Fig. 6** and **S2**) suggests that assaying linked SFK and p38 phosphorylation might be useful when screening NRP1-targeting compounds for their ability to modulate the neurovascular barrier, particularly when evaluating CendR-based drugs intended to treat human disease. Further, observing similar permeability signalling in mouse, rat and human ECs in response to EG00229 (**Figs. 4, 6** and **S2**) corroborates that rodent ECs are likely relevant for modelling signalling events at the neurovascular barrier, as proposed [37,48,61].

Although chronic increases in vascular leakage pose a significant clinical problem in ischemic conditions of the brain and retina, the *ex vivo* retina model measures specifically acute paracellular permeability induction. Further work is thus needed to determine whether cumulative effects of prolonged EG00229 treatment would translate into clinically relevant neurovascular barrier modulation, such as oedema due to chronic VEGF164 upregulation. Thus, it should be investigated whether EG00229's ability to open the neurovascular barrier might enhance drug penetration into cells or across vascular barriers, in analogy to the benefit of multivalent CendR peptide-coated particles, which promote the transportation of payloads deep into extravascular tissue [11].

References

1. Schwarz Q, Ruhrberg C (2010) Neuropilin, you gotta let me know: should I stay or should I go? Cell Adhesion & Migration 4 (1):61-66
2. Plein A, Fantin A, Ruhrberg C (2014) Neuropilin regulation of angiogenesis, arteriogenesis, and vascular permeability. Microcirculation 21 (4):315-323. doi:10.1111/micc.12124
3. Acevedo LM, Barillas S, Weis SM, Gothert JR, Cheresh DA (2008) Semaphorin 3A suppresses VEGF-mediated angiogenesis yet acts as a vascular permeability factor. Blood 111 (5):2674-2680. doi:blood-2007-08-110205 [pii] 10.1182/blood-2007-08-110205
4. Raimondi C, Ruhrberg C (2013) Neuropilin signalling in vessels, neurons and tumours. Seminars in Cell & Developmental Biology 24 (3):172-178. doi:10.1016/j.semcdb.2013.01.001
5. Domingues A, Fantin A (2021) Neuropilin 1 Regulation of Vascular Permeability Signaling. Biomolecules 11 (5). doi:10.3390/biom11050666
6. Chaudhary B, Khaled YS, Ammori BJ, Elkord E (2014) Neuropilin 1: function and therapeutic potential in cancer. Cancer Immunol Immunother 63 (2):81-99. doi:10.1007/s00262-013-1500-0
7. Chuckran CA, Liu C, Bruno TC, Workman CJ, Vignali DA (2020) Neuropilin-1: a checkpoint target with unique implications for cancer immunology and immunotherapy. J Immunother Cancer 8 (2). doi:10.1136/jitc-2020-000967

471 8. Liang WC, Dennis MS, Stawicki S, Chanthery Y, Pan Q, Chen Y, Eigenbrot C, Yin J, Koch AW,
472 Wu X, Ferrara N, Bagri A, Tessier-Lavigne M, Watts RJ, Wu Y (2007) Function blocking
473 antibodies to neuropilin-1 generated from a designed human synthetic antibody phage library. J
474 Mol Biol 366 (3):815-829. doi:S0022-2836(06)01550-6 [pii] 10.1016/j.jmb.2006.11.021
475 9. Pan Q, Chanthery Y, Liang WC, Stawicki S, Mak J, Rathore N, Tong RK, Kowalski J, Yee SF,
476 Pacheco G, Ross S, Cheng Z, Le Couter J, Plowman G, Peale F, Koch AW, Wu Y, Bagri A,
477 Tessier-Lavigne M, Watts RJ (2007) Blocking neuropilin-1 function has an additive effect with
478 anti-VEGF to inhibit tumor growth. Cancer Cell 11 (1):53-67. doi:S1535-6108(06)00367-9 [pii]
479 10.1016/j.ccr.2006.10.018
480 10. Zanuy D, Kotla R, Nussinov R, Teesalu T, Sugahara KN, Aleman C, Haspel N (2013) Sequence
481 dependence of C-end rule peptides in binding and activation of neuropilin-1 receptor. J Struct Biol
482 182 (2):78-86. doi:10.1016/j.jsb.2013.02.006
483 11. Teesalu T, Sugahara KN, Kotamraju VR, Ruoslahti E (2009) C-end rule peptides mediate
484 neuropilin-1-dependent cell, vascular, and tissue penetration. Proceedings of the National
485 Academy of Sciences of the United States of America 106 (38):16157-16162. doi:10.1073/
486 pnas.0908201106
487 12. Roth L, Prahst C, Ruckdeschel T, Savant S, Westrom S, Fantin A, Riedel M, Heroult M, Ruhrberg
488 C, Augustin HG (2016) Neuropilin-1 mediates vascular permeability independently of vascular
489 endothelial growth factor receptor-2 activation. Sci Signal 9 (425):ra42.
490 doi:10.1126/scisignal.aad3812
491 13. Daly JL, Simonetti B, Klein K, Chen KE, Williamson MK, Anton-Plagaro C, Shoemark DK, Simon-
492 Gracia L, Bauer M, Hollandi R, Greber UF, Horvath P, Sessions RB, Helenius A, Hiscox JA,
493 Teesalu T, Matthews DA, Davidson AD, Collins BM, Cullen PJ, Yamauchi Y (2020) Neuropilin-1
494 is a host factor for SARS-CoV-2 infection. Science 370 (6518):861-865.
495 doi:10.1126/science.abd3072
496 14. Kolaric A, Jukic M, Bren U (2022) Novel Small-Molecule Inhibitors of the SARS-CoV-2 Spike
497 Protein Binding to Neuropilin 1. Pharmaceuticals (Basel) 15 (2). doi:10.3390/ph15020165
498 15. Jia H, Bagherzadeh A, Hartzoulakis B, Jarvis A, Lohr M, Shaikh S, Aqil R, Cheng L, Tickner M,
499 Esposito D, Harris R, Driscoll PC, Selwood DL, Zachary IC (2006) Characterization of a bicyclic
500 peptide neuropilin-1 (NP-1) antagonist (EG3287) reveals importance of vascular endothelial
501 growth factor exon 8 for NP-1 binding and role of NP-1 in KDR signaling. The Journal of biological
502 chemistry 281 (19):13493-13502. doi:10.1074/jbc.M512121200
503 16. Peng K, Li Y, Bai Y, Jiang T, Sun H, Zhu Q, Xu Y (2020) Discovery of novel nonpeptide small-
504 molecule NRP1 antagonists: Virtual screening, molecular simulation and structural modification.
505 Bioorg Med Chem 28 (1):115183. doi:10.1016/j.bmc.2019.115183
506 17. Powell J, Mota F, Steadman D, Soudy C, Miyauchi JT, Crosby S, Jarvis A, Reisinger T, Winfield
507 N, Evans G, Finniear A, Yelland T, Chou YT, Chan AWE, O'Leary A, Cheng L, Liu D, Fotinou C,
508 Milagre C, Martin JF, Jia H, Frankel P, Djordjevic S, Tsirka SE, Zachary IC, Selwood DL (2018)

509 Small Molecule Neuropilin-1 Antagonists Combine Antiangiogenic and Antitumor Activity with
510 Immune Modulation through Reduction of Transforming Growth Factor Beta (TGFbeta)
511 Production in Regulatory T-Cells. J Med Chem 61 (9):4135-4154.
512 doi:10.1021/acs.jmedchem.8b00210
513 18. Jarvis A, Allerston CK, Jia H, Herzog B, Garza-Garcia A, Winfield N, Ellard K, Aqil R, Lynch R,
514 Chapman C, Hartzoulakis B, Nally J, Stewart M, Cheng L, Menon M, Tickner M, Djordjevic S,
515 Driscoll PC, Zachary I, Selwood DL (2010) Small molecule inhibitors of the neuropilin-1 vascular
516 endothelial growth factor A (VEGF-A) interaction. Journal of Medicinal Chemistry 53 (5):2215-
517 2226. doi:10.1021/jm901755g
518 19. Huang Z, Cheng C, Xiong H, Wang Y, Chen KK, Yang J, Xiao B, Zhang R, Li S, Sang Y (2018)
519 NRP1 promotes cell migration and invasion and serves as a therapeutic target in nasopharyngeal
520 carcinoma. Int J Clin Exp Pathol 11 (5):2460-2469
521 20. Zheng C, Wang H, Zhao S, Ma C, Gao H, Yang F, Zhou X, Lu J, Zhang C, Zhu H (2022) Inhibition
522 of neuropilin-1 enhances the therapeutic effects of lenvatinib in suppressing cholangiocarcinoma
523 cells via the c-Met pathway. Eur J Pharmacol 935:175290. doi:10.1016/j.ejphar.2022.175290
524 21. Miyauchi JT, Chen D, Choi M, Nissen JC, Shroyer KR, Djordevic S, Zachary IC, Selwood D,
525 Tsirka SE (2016) Ablation of Neuropilin 1 from glioma-associated microglia and macrophages
526 slows tumor progression. Oncotarget 7 (9):9801-9814. doi:10.18632/oncotarget.6877
527 22. Moutal A, Martin LF, Boinon L, Gomez K, Ran D, Zhou Y, Stratton HJ, Cai S, Luo S, Gonzalez
528 KB, Perez-Miller S, Patwardhan A, Ibrahim MM, Khanna R (2021) SARS-CoV-2 spike protein co-
529 opts VEGF-A/neuropilin-1 receptor signaling to induce analgesia. Pain 162 (1):243-252.
530 doi:10.1097/j.pain.0000000000002097
531 23. Napolitano V, Tamagnone L (2019) Neuropilins Controlling Cancer Therapy Responsiveness.
532 Int J Mol Sci 20 (8). doi:10.3390/ijms20082049
533 24. Raimondi C, Brash JT, Fantin A, Ruhrberg C (2016) NRP1 function and targeting in
534 neurovascular development and eye disease. Prog Retin Eye Res 52:64-83.
535 doi:10.1016/j.preteyeres.2016.02.003
536 25. Mercurio AM (2019) VEGF/Neuropilin Signaling in Cancer Stem Cells. Int J Mol Sci 20 (3).
537 doi:10.3390/ijms20030490
538 26. Gu C, Rodriguez ER, Reimert DV, Shu T, Fritzsch B, Richards LJ, Kolodkin AL, Ginty DD (2003)
539 Neuropilin-1 conveys semaphorin and VEGF signaling during neural and cardiovascular
540 development. Dev Cell 5 (1):45-57
541 27. Okabe K, Kobayashi S, Yamada T, Kurihara T, Tai-Nagara I, Miyamoto T, Mukouyama YS, Sato
542 TN, Suda T, Ema M, Kubota Y (2014) Neurons limit angiogenesis by titrating VEGF in retina. Cell
543 159 (3):584-596. doi:10.1016/j.cell.2014.09.025
544 28. Ho VC, Duan LJ, Cronin C, Liang BT, Fong GH (2012) Elevated vascular endothelial growth
545 factor receptor-2 abundance contributes to increased angiogenesis in vascular endothelial growth
546 factor receptor-1-deficient mice. Circulation 126 (6):741-752.

547 doi:10.1161/CIRCULATIONAHA.112.091603
548 29. Fantin A, Schwarz Q, Davidson K, Normando EM, Denti L, Ruhrberg C (2011) The cytoplasmic
549 domain of neuropilin 1 is dispensable for angiogenesis, but promotes the spatial separation of
550 retinal arteries and veins. Development 138 (19):4185-4191. doi:10.1242/dev.070037
551 30. Fantin A, Lampropoulou A, Senatore V, Brash JT, Prahst C, Lange CA, Liyanage SE, Raimondi
552 C, Bainbridge JW, Augustin HG, Ruhrberg C (2017) VEGF165-induced vascular permeability
553 requires NRP1 for ABL-mediated SRC family kinase activation. J Exp Med 214 (4):1049-1064.
554 doi:10.1084/jem.20160311
555 31. Dragoni S, Caridi B, Karatsai E, Burgoyne T, Sarker MH, Turowski P (2021) AMP-activated
556 protein kinase is a key regulator of acute neurovascular permeability. J Cell Sci 134 (7).
557 doi:10.1242/jcs.253179
558 32. Hudson N, Powner MB, Sarker MH, Burgoyne T, Campbell M, Ockrim ZK, Martinelli R, Futter
559 CE, Grant MB, Fraser PA, Shima DT, Greenwood J, Turowski P (2014) Differential apicobasal
560 VEGF signaling at vascular blood-neural barriers. Dev Cell 30 (5):541-552.
561 doi:10.1016/j.devcel.2014.06.027
562 33. Parker MW, Xu P, Li X, Vander Kooi CW (2012) Structural basis for selective vascular endothelial
563 growth factor-A (VEGF-A) binding to neuropilin-1. The Journal of Biological Chemistry 287
564 (14):11082-11089. doi:10.1074/jbc.M111.331140
565 34. DeLano W (2002) The PyMOL Molecular Graphics System (2002) DeLano Scientific, Palo Alto,
566 CA, USA. http://www.pymol.org.
567 35. Laskowski RA, Swindells MB (2011) LigPlot+: multiple ligand-protein interaction diagrams for
568 drug discovery. J Chem Inf Model 51 (10):2778-2786. doi:10.1021/ci200227u
569 36. Martins T, Burgoyne T, Kenny BA, Hudson N, Futter CE, Ambrosio AF, Silva AP, Greenwood J,
570 Turowski P (2013) Methamphetamine-induced nitric oxide promotes vesicular transport in blood-
571 brain barrier endothelial cells. Neuropharmacology 65:74-82.
572 doi:10.1016/j.neuropharm.2012.08.021
573 37. Weksler B, Romero IA, Couraud PO (2013) The hCMEC/D3 cell line as a model of the human
574 blood brain barrier. Fluids Barriers CNS 10 (1):16. doi:10.1186/2045-8118-10-16
575 38. Fuh G, Garcia KC, de Vos AM (2000) The interaction of neuropilin-1 with vascular endothelial
576 growth factor and its receptor flt-1. The Journal of Biological Chemistry 275 (35):26690-26695.
577 doi:10.1074/jbc.M003955200
578 39. Benhadou F, Glitzner E, Brisebarre A, Swedlund B, Song Y, Dubois C, Rozzi M, Paulissen C,
579 Del Marmol V, Sibilia M, Blanpain C (2020) Epidermal autonomous VEGFA/Flt1/Nrp1 functions
580 mediate psoriasis-like disease. Sci Adv 6 (2):eaax5849. doi:10.1126/sciadv.aax5849
581 40. Takahashi H, Hattori S, Iwamatsu A, Takizawa H, Shibuya M (2004) A novel snake venom
582 vascular endothelial growth factor (VEGF) predominantly induces vascular permeability through
583 preferential signaling via VEGF receptor-1. J Biol Chem 279 (44):46304-46314.
584 doi:10.1074/jbc.M403687200

585 41. Gelfand MV, Hagan N, Tata A, Oh WJ, Lacoste B, Kang KT, Kopycinska J, Bischoff J, Wang JH,
586 Gu C (2014) Neuropilin-1 functions as a VEGFR2 co-receptor to guide developmental
587 angiogenesis independent of ligand binding. Elife 3:e03720. doi:10.7554/eLife.03720
588 42. Prahst C, Heroult M, Lanahan AA, Uziel N, Kessler O, Shraga-Heled N, Simons M, Neufeld G,
589 Augustin HG (2008) Neuropilin-1-VEGFR-2 complexing requires the PDZ-binding domain of
590 neuropilin-1. J Biol Chem 283 (37):25110-25114. doi:C800137200 [pii] 10.1074/jbc.C800137200
591 43. Lanahan A, Zhang X, Fantin A, Zhuang Z, Rivera-Molina F, Speichinger K, Prahst C, Zhang J,
592 Wang Y, Davis G, Toomre D, Ruhrberg C, Simons M (2013) The Neuropilin 1 Cytoplasmic
593 Domain Is Required for VEGF-A-Dependent Arteriogenesis. Developmental Cell 25 (2):156-168.
594 doi:10.1016/j.devcel.2013.03.019
595 44. Herzog B, Pellet-Many C, Britton G, Hartzoulakis B, Zachary IC (2011) VEGF binding to NRP1
596 is essential for VEGF stimulation of endothelial cell migration, complex formation between NRP1
597 and VEGFR2, and signaling via FAK Tyr407 phosphorylation. Molecular Biology of the Cell 22
598 (15):2766-2776. doi:10.1091/mbc.E09-12-1061
599 45. Eliceiri BP, Paul R, Schwartzberg PL, Hood JD, Leng J, Cheresh DA (1999) Selective
600 requirement for Src kinases during VEGF-induced angiogenesis and vascular permeability. Mol
601 Cell 4 (6):915-924. doi:S1097-2765(00)80221-X [pii]
602 46. Zhu X, Kim JL, Newcomb JR, Rose PE, Stover DR, Toledo LM, Zhao H, Morgenstern KA (1999)
603 Structural analysis of the lymphocyte-specific kinase Lck in complex with non-selective and Src
604 family selective kinase inhibitors. Structure 7 (6):651-661. doi:10.1016/s0969-2126(99)80086-0
605 47. Sun Z, Li X, Massena S, Kutschera S, Padhan N, Gualandi L, Sundvold-Gjerstad V, Gustafsson
606 K, Choy WW, Zang G, Quach M, Jansson L, Phillipson M, Abid MR, Spurkland A, Claesson-
607 Welsh L (2012) VEGFR2 induces c-Src signaling and vascular permeability in vivo via the adaptor
608 protein TSAd. The Journal of Experimental Medicine 209 (7):1363-1377.
609 doi:10.1084/jem.20111343
610 48. Qi D, Lin H, Hu B, Wei Y (2023) A review on in vitro model of the blood-brain barrier (BBB) based
611 on hCMEC/D3 cells. J Control Release 358:78-97. doi:10.1016/j.jconrel.2023.04.020
612 49. Orsenigo F, Giampietro C, Ferrari A, Corada M, Galaup A, Sigismund S, Ristagno G, Maddaluno
613 L, Koh GY, Franco D, Kurtcuoglu V, Poulikakos D, Baluk P, McDonald D, Grazia Lampugnani M,
614 Dejana E (2012) Phosphorylation of VE-cadherin is modulated by haemodynamic forces and
615 contributes to the regulation of vascular permeability in vivo. Nature Communications 3:1208.
616 doi:10.1038/ncomms2199
617 50. Thibeault S, Rautureau Y, Oubaha M, Faubert D, Wilkes BC, Delisle C, Gratton JP (2010) S-
618 nitrosylation of beta-catenin by eNOS-derived NO promotes VEGF-induced endothelial cell
619 permeability. Mol Cell 39 (3):468-476. doi:10.1016/j.molcel.2010.07.013
620 51. Esser S, Lampugnani MG, Corada M, Dejana E, Risau W (1998) Vascular endothelial growth
621 factor induces VE-cadherin tyrosine phosphorylation in endothelial cells. J Cell Sci 111 (Pt
622 13):1853-1865. doi:10.1242/jcs.111.13.1853

623 52. Gavard J, Gutkind JS (2006) VEGF controls endothelial-cell permeability by promoting the beta-
624 arrestin-dependent endocytosis of VE-cadherin. Nat Cell Biol 8 (11):1223-1234.
625 doi:10.1038/ncb1486
626 53. Vander Kooi CW, Jusino MA, Perman B, Neau DB, Bellamy HD, Leahy DJ (2007) Structural
627 basis for ligand and heparin binding to neuropilin B domains. Proceedings of the National
628 Academy of Sciences of the United States of America 104 (15):6152-6157.
629 doi:10.1073/pnas.0700043104
630 54. Goudiaby I, Malliavin TE, Mocchetti E, Mathiot S, Acherar S, Frochot C, Barberi-Heyob M, Guillot
631 B, Favier F, Didierjean C, Jelsch C (2023) New Crystal Form of Human Neuropilin-1 b1 Fragment
632 with Six Electrostatic Mutations Complexed with KDKPPR Peptide Ligand. Molecules 28 (14).
633 doi:10.3390/molecules28145603
634 55. O'Leary F, Campbell M (2023) The blood-retina barrier in health and disease. FEBS J 290
635 (4):878-891. doi:10.1111/febs.16330
636 56. Dragoni S, Turowski P (2018) Polarised VEGFA Signalling at Vascular Blood-Neural Barriers.
637 Int J Mol Sci 19 (5). doi:10.3390/ijms19051378
638 57. Kawamura H, Li X, Goishi K, van Meeteren LA, Jakobsson L, Cebe-Suarez S, Shimizu A, Edholm
639 D, Ballmer-Hofer K, Kjellen L, Klagsbrun M, Claesson-Welsh L (2008) Neuropilin-1 in regulation
640 of VEGF-induced activation of p38MAPK and endothelial cell organization. Blood 112 (9):3638-
641 3649. doi:10.1182/blood-2007-12-125856
642 58. Grun D, Adhikary G, Eckert RL (2019) NRP-1 interacts with GIPC1 and SYX to activate p38
643 MAPK signaling and cancer stem cell survival. Mol Carcinog 58 (4):488-499.
644 doi:10.1002/mc.22943
645 59. Ninchoji T, Love DT, Smith RO, Hedlund M, Vestweber D, Sessa WC, Claesson-Welsh L (2021)
646 eNOS-induced vascular barrier disruption in retinopathy by c-Src activation and tyrosine
647 phosphorylation of VE-cadherin. Elife 10. doi:10.7554/eLife.64944
648 60. Weis S, Shintani S, Weber A, Kirchmair R, Wood M, Cravens A, McSharry H, Iwakura A, Yoon
649 YS, Himes N, Burstein D, Doukas J, Soll R, Losordo D, Cheresh D (2004) Src blockade stabilizes
650 a Flk/cadherin complex, reducing edema and tissue injury following myocardial infarction. The
651 Journal of Clinical Investigation 113 (6):885-894. doi:10.1172/JCI20702
652 61. Sanchez-Dengra B, Gonzalez-Alvarez I, Sousa F, Bermejo M, Gonzalez-Alvarez M, Sarmento
653 B (2021) In vitro model for predicting the access and distribution of drugs in the brain using
654 hCMEC/D3 cells. Eur J Pharm Biopharm 163:120-126. doi:10.1016/j.ejpb.2021.04.002
655

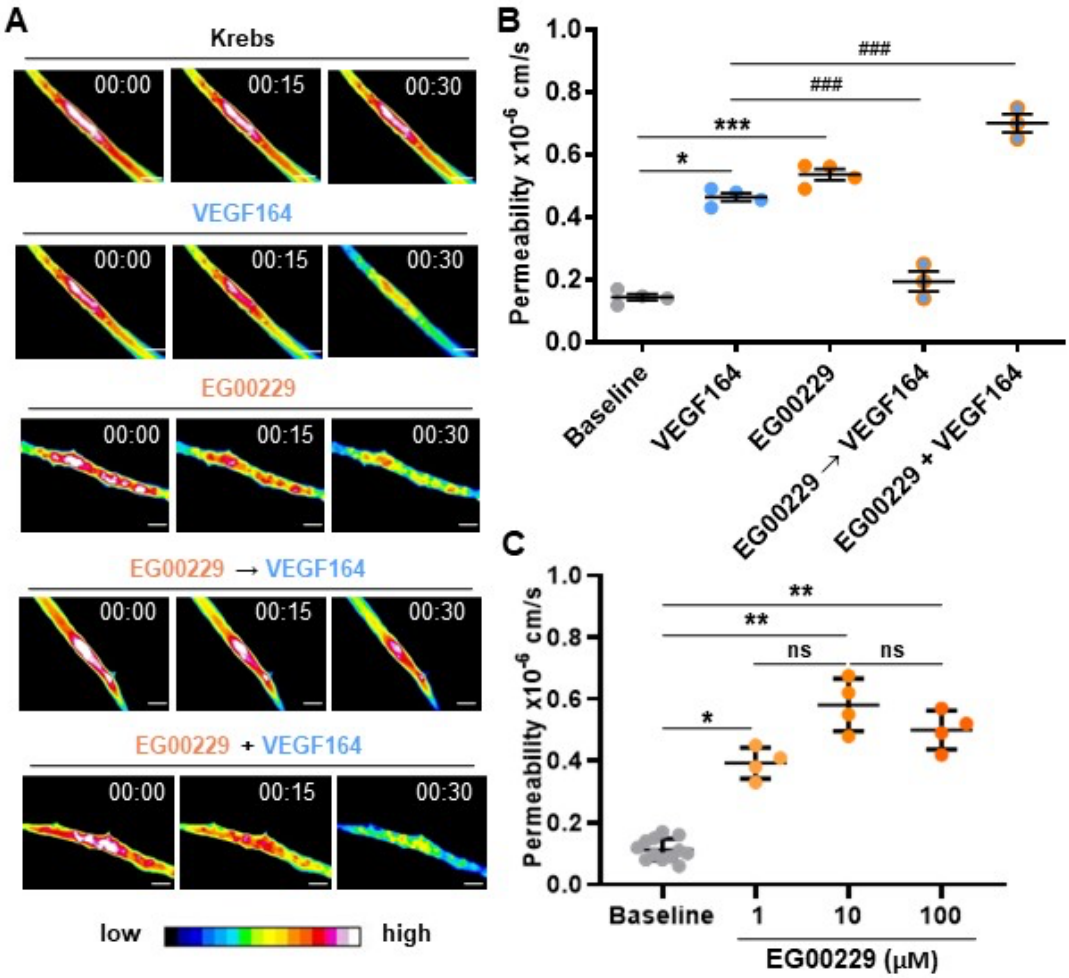

Figure 1 *EG00229 induces retinal vascular leakage*

(**A**) Representative 16-color pseudocoloured images of fluorescence intensity in vessel segments of wild type *ex vivo* retina at the indicated times after treatment with vehicle (Krebs) or VEGF164 and/or EG00229 as indicated.

(**B,C**) Quantification of fluorescence changes over 2 min compared to baseline (vehicle), after (**B**) treatment with EG00229 (n = 4), VEGF164 (n = 4), VEGF164 after EG00229 pre-treatment (n = 3) or co-treatment of EG00229 and VEGF164 (n = 3), or after (**C**) treatment with different EG00229 concentrations (n = 4 each). Data are shown as mean ± SD. Each data point indicates the value for one retina from one mouse after one instance of adding a test substance. Repeated measures one-way ANOVA followed by post-hoc Dunnett's test; asterisks: significant P-values for test substance compared to baseline: * $P < 0.05$, ** $P < 0.01$,*** $P < 0.001$; hashtags: significant P-values for test substance(s) compared to VEGF164: ### $P < 0.001$; ns, not significant ($P > 0.05$).

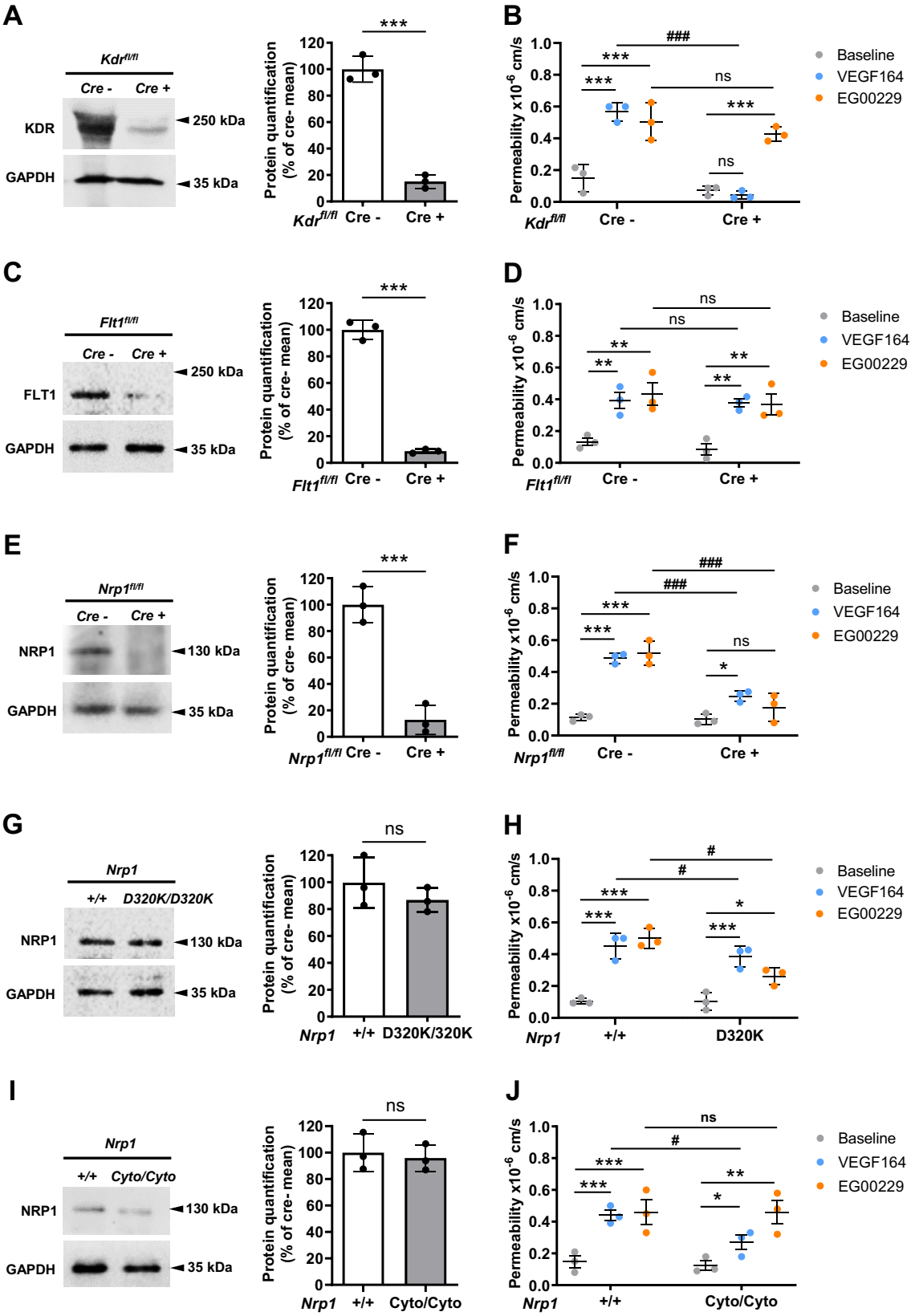

Figure 2 *EG00229 induces retinal vascular leakage via NRP1, independently of KDR and FLT1*

(**A-F**) EG00229-induced retinal vascular leakage depends on endothelial NRP1, but not VEGFR2 or VEGFR1. Adult *Kdr*$^{fl/fl}$ (**A,B**), *Flt1*$^{fl/fl}$ (**C,D**) and *Nrp1*$^{fl/fl}$ (**E,F**) mice expressing or lacking *Cdh5*-CreER^{T2} were tamoxifen-treated and used two weeks after the last tamoxifen dose for lung immunoblotting

with the indicated antibodies (**A,C,E**) and *ex vivo* retina permeability assays (**B,D,F**).

(**G-J**) EG00229-induced retinal vascular leakage depends on NRP1's CendR but not cytoplasmic domain. Immunoblotting of lung lysates with the indicated antibodies (**G,H**) and *ex vivo* retina permeability assays (**I,J**) in *Nrp1*$^{D320K/D320K}$ (**E,F,H**) and *Nrp1*$^{cyto/cyto}$ (**I,J**) mice.

In all experiments, mice were used as tissue donors for parallel lung immunoblotting to determine receptor protein levels and permeability assays with one retina per mouse to determine the genotype effect on VEGF164- versus EG00229-induced vascular leakage; n = 3 mice for each genotype (the second retina was used for experiments shown in Figure 3). The migration of the molecular weight marker is indicated with arrowheads to the left of each immunoblot.

Lung immunoblotting: Data are shown as mean ± SD; each data point indicates the value for one retina from one mouse. Asterisks indicate significant P-values for changes in the level of the indicated proteins (unpaired Student's t-test): *, $P < 0.05$; **, $P < 0.01$; ***, $P < 0.001$; ns, not significant ($P > 0.05$).

Ex vivo retinal permeability assay: For repeated testing of the same retina, the order of adding VEGF164 or EG00229 was alternated, with washing each time in Krebs solution for 10 min followed by recording the new baseline. Data are shown as mean ± SD; each data point indicates the value for one retina from one mouse, whereby all recordings for one agent in one retina were averaged to obtain the value for that retina. Significant P-values are shown for fluorescence changes induced by VEGF164 or EG00229 versus Krebs for specific genotypes (asterisks) and in mutants versus controls (hashtags: *, $P < 0.05$; **, $P < 0.01$; ***, $P < 0.001$; #, $P < 0.05$; ##, $P < 0.01$; ns, not significant ($P > 0.05$). Repeated measures two-way ANOVA.

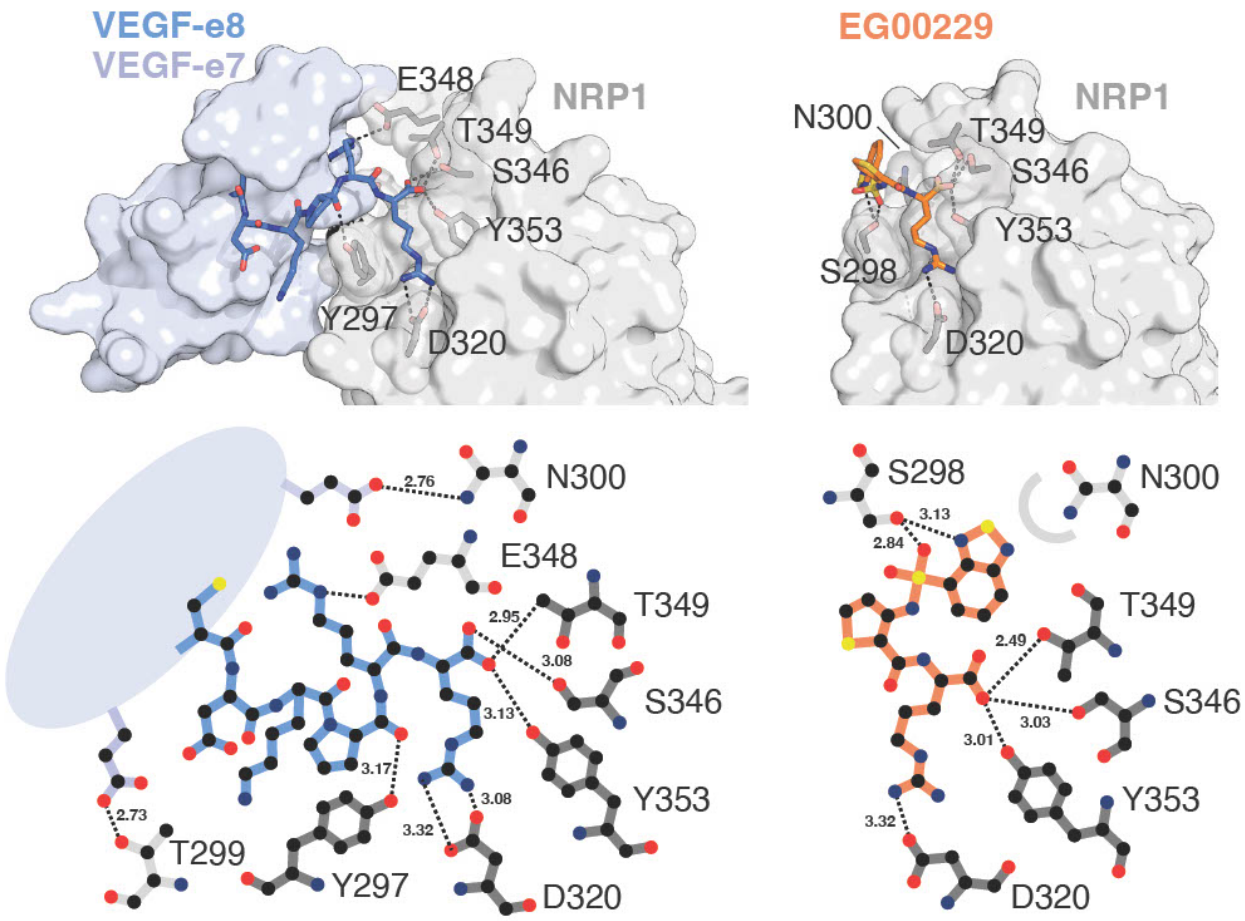

Figure 3 *VEGF165 and EG00229 bind similarly to the NRP1 b1 domain*

Schematic representation of the crystal structures (**A,B**) and corresponding interaction diagrams (**C,D**) of the NRP1 b1 domain in complex with VEGF165 exon 7-8 (PDB:4deq; **A,C**) or the NRP1 b1 domain with EG00229 (PDB:3i97; **B,D**). Key interacting NRP1 residues are shown with stick representation with corresponding hydrogen bonds as black dashes. A stacking interaction is represented by a semi-circle in (**B)**.

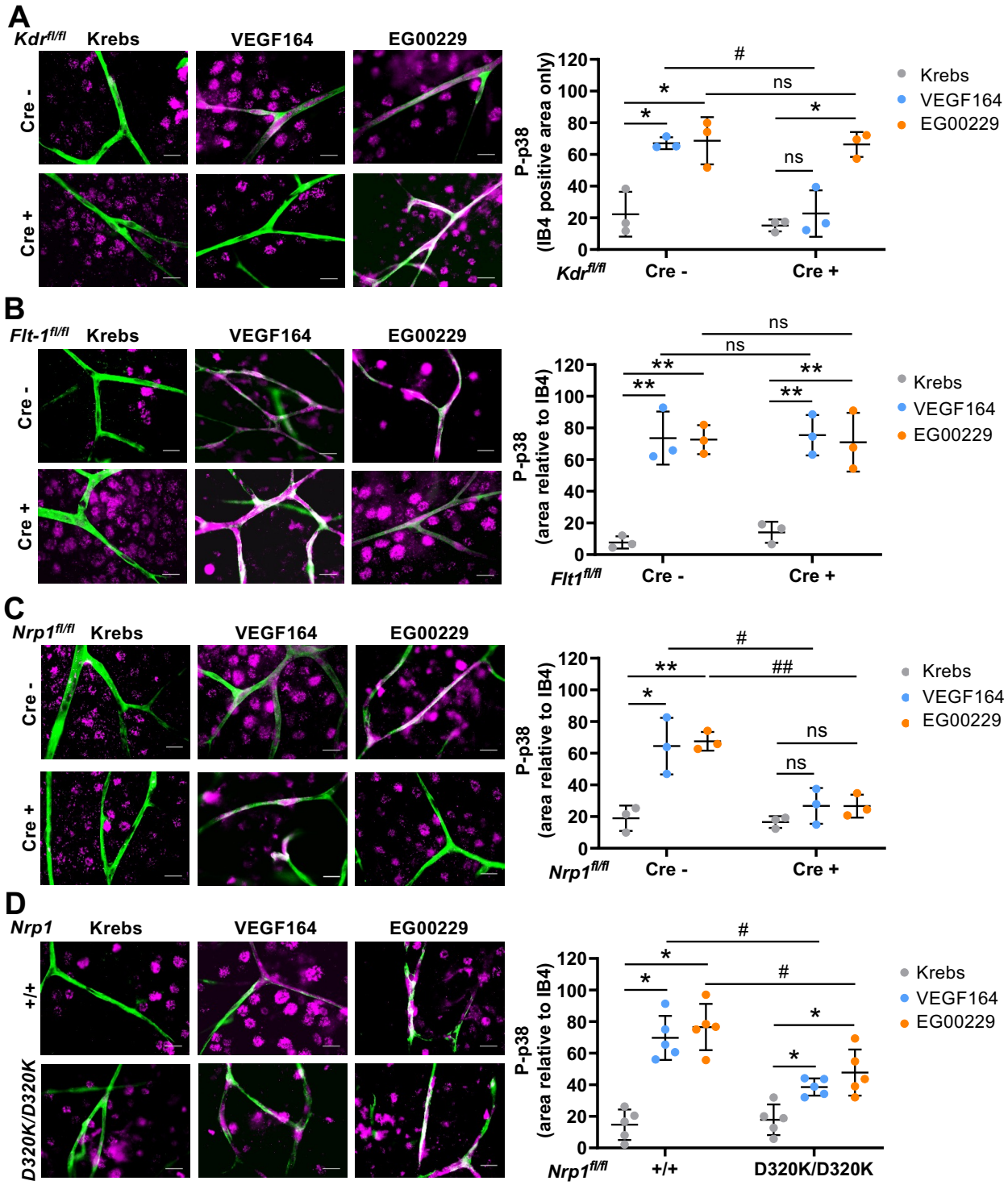

Figure 4 *EG00229 activates p38 in retinal vasculature through NRP1's, independently of KDR and FLT1*

Freshly dissected retinae from mice of the indicated genotypes were incubated in Krebs solution with or without VEGF164 or EG00229, fixed and immunostained with the vascular EC marker isolectin B4 (green) and an antibody against P-p38 (magenta). tinas were obtained from the second eye of mice used for *ex vivo* permeability experiments in Figure 2. In (**A-C**), we used retinas from adult *Kdr*$^{fl/fl}$ (**A**), *Flt1*$^{fl/fl}$ (**B**) and *Nrp1*$^{fl/fl}$ (**C**) mice expressing or lacking the endothelial *Cdh5*-CreER^{T2}

transgene, which had been tamoxifen-treated two weeks before *ex vivo* treatment of the retina. In (**D**), we used retinas from *Nrp1*$^{D320K/D320K}$ and wild type littermate mice for *ex vivo* treatment. Re

Epifluorescent images (scale bars: 10 µm) show P-p38 in IB4-positive vasculature and IB4-negative neuroglial cells. Epifluorescent images were then used for quantification of P-p38 pixel intensity in the IB4-positive area. Data are shown as mean ± SD; each data point represents the value for one retina from one mouse; n = 3 mice for each genotype. Significant P-values are shown for P-p38 staining area for VEGF164 or EG00229 versus vehicle (Krebs) for each genotype (asterisks) and for VEGF164 or EG00229 in mutant versus control (hashtags) (two-way ANOVA): *, $P < 0.05$; **, $P < 0.01$; ***, $P < 0.001$; #, $P < 0.05$; ns, not significant ($P > 0.05$).

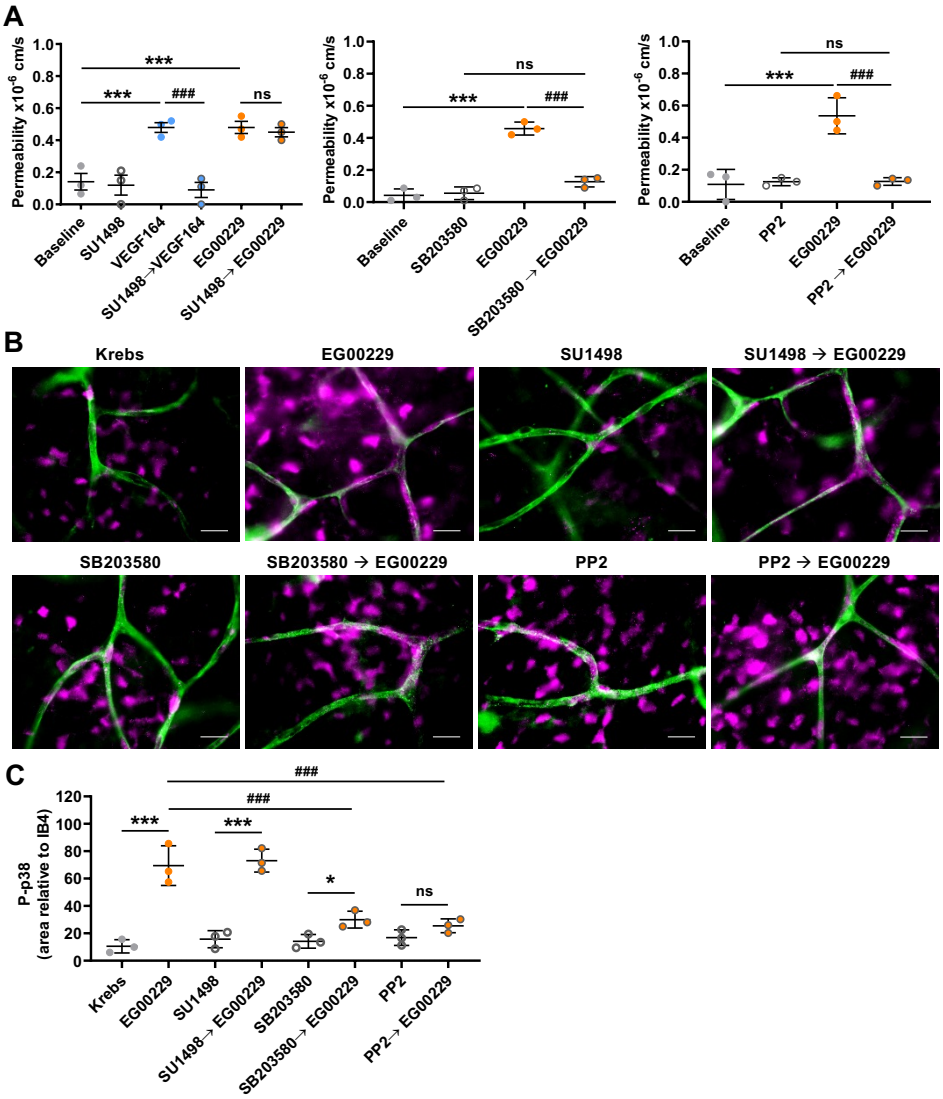

Figure 5 *EG00229 induces retinal vascular leakage via p38 and SFK activation*

(**A**) Quantification of sulforhodamine B fluorescence changes in the *ex vivo* retina permeability assay after treatment with SU1498, SB203580 or PP2 (inhibitors) alone, compared to VEGF164 or EG00229 treatment with or without inhibitor pre-treatment (n = 3 treatments of 3 independent retinas each). Data are shown as mean ± SD; each data point represents the value for one retina from one mouse. Significant P-values are shown for inhibitor versus baseline (asterisks) and EG00229 ± inhibitor (hashtags): *** P, < 0.001; ###, P < 0.001; ns, not significant (P > 0.05). Repeated measures one-way ANOVA.

(**B,C**) Freshly dissected retinae from wild type mice were incubated in Krebs solution (vehicle) with or without EG00229, or preincubated with SB203580 or PP2 for 15 min before adding EG00229. *Ex vivo* retinae were then fixed and immunostained with the vascular EC marker isolectin B4 (IB4, green) and an antibody against P-p38 (magenta). Epifluorescent images (**B**, scale bars: 10 µm) were used for quantification of pixel intensity for P-p38 in the IB4-positive vascular area (**C**). Significant P-values for P-p38 staining in the IB4+ area for inhibitors (SB203580 or PP2 versus SB203580) versus EG00229 are indicated with asterisks or after pre-treatment with the inhibitors, indicated with hashtags: *, P < 0.05; ***, P < 0.001; ###, P < 0.001; ns, not significant (P > 0.05); one-way ANOVA.

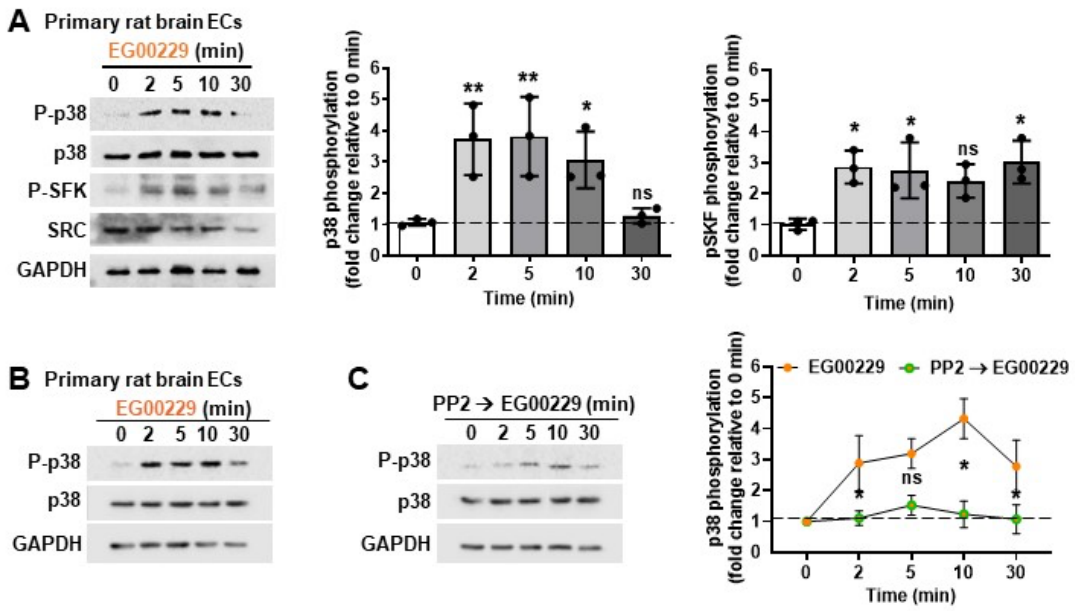

Figure 6 *EG00229 induces paracellular permeability signalling in rat brain ECs*

Confluent primary rat brain ECs were treated with EG00229 for the indicated times. Cell lysates were used for immunoblotting with the indicated antibodies, followed by quantification of pixel intensities for P-p38 and P-SFK relative to total p38 and SRC pixel intensities, respectively. GAPDH was used as a loading control. In (**A**), p38 and SFK phosphorylation levels after EG0229 treatment were quantified at different time points relative to 0 min. In (**B**), EG00229 treatment was preceded by incubation with PP2; decreased EG00229-induced p38 phosphorylation after PP2 treatment was compared to EG00229 alone at each time point. Data are shown as mean fold change ± SD. Asterisks indicate significant P-values for phosphorylation induction after EG00229 treatment (: *, $P < 0.05$; **, $P < 0.01$; ns, not significant ($P > 0.05$); one-way ANOVA.

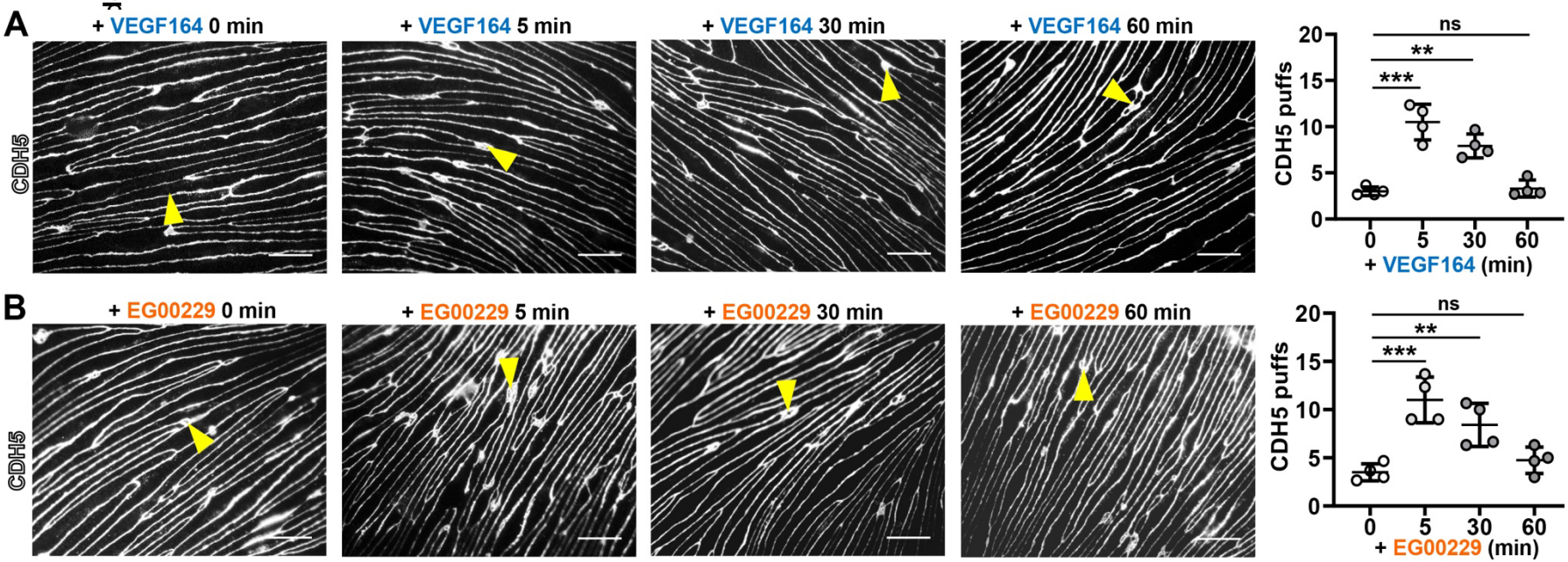

Figure 7 *EG00229 causes junctional remodelling in brain microvascular EC monolayers*

Epifluorescence images of confluent primary rat brain ECs for CDH5 fixed were immunostained at the indicated times after VEGF164 (**A**) or EG00229 (**B**) treatment; scale bars: 100 µm. Yellow arrowheads indicate broad CDH5 staining ('puffs'). Quantification of puff number: data show the mean ± SD from 4 independent primary cell preparations; each data point represents the average of 3 transwells (technical repeats). Asterisks indicate significant P-values for the number of puffs compared to 0 min (one-way ANOVA): ** $P < 0.01$; *** $P < 0.001$; ns, not significant ($P > 0.05$

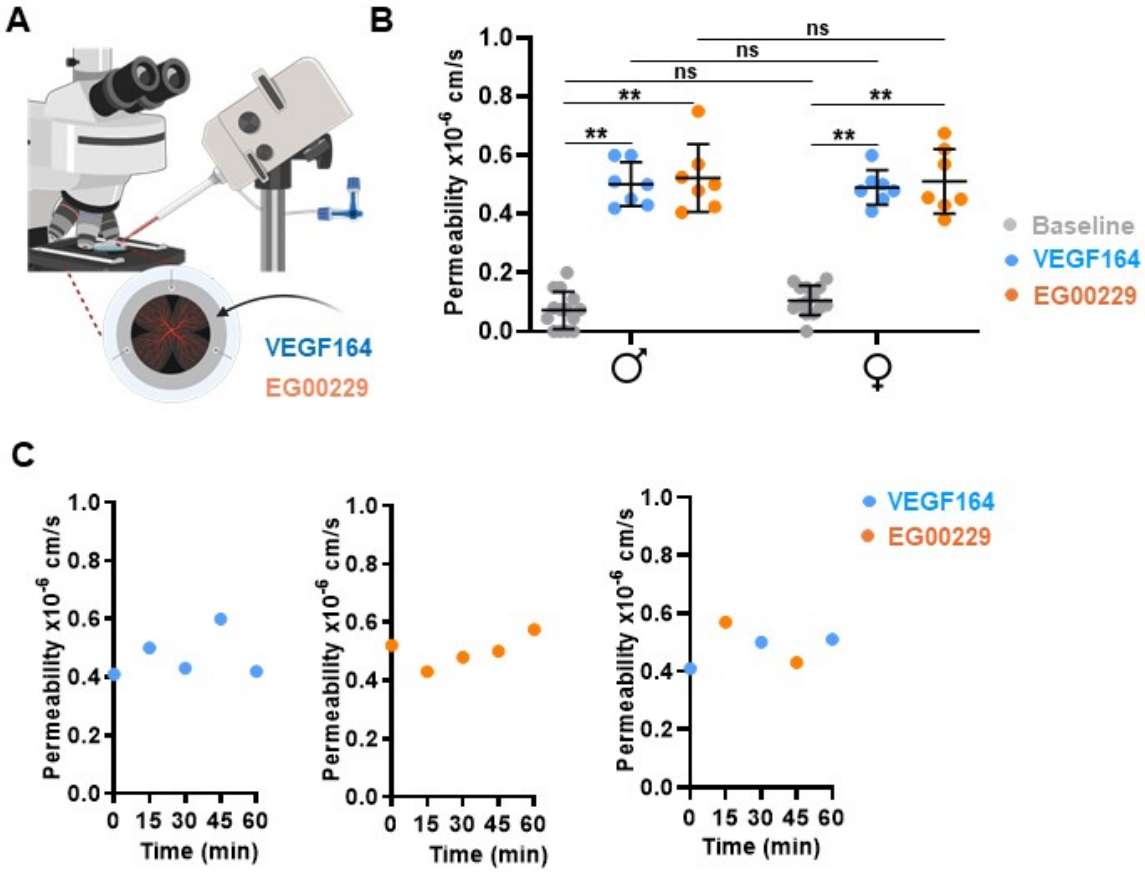

Figure S1. *EG00229 increases retinal microvascular EC permeability similar to VEGF164.*

(**A**) Schematic representation of the *ex vivo* retinal permeability assay.

(**B,C**) Quantification of retinal vascular leakage in the *ex vivo* retinal vascular permeability assay after adding EG00229 or VEGF164 in retinae of (**B**) male and female wildtype mice (n = 7 each) and (**C**) after repeated addition of VEGF164 and EG00229 to the same retinal vessel, or when added alternately; for repeated testing, the retina was washed with Krebs for 10 min and a new baseline recorded. Data are shown as mean ± SD. Each data point indicates the value for the fluorescence change in one retina from one mouse obtained 2 min after one instance of adding a test substance. Repeated measures two-way ANOVA followed by post-hoc Dunnett's test: asterisks indicate significant P-values for test substance addition compared to baseline (Krebs); *, $P < 0.05$; **, $P < 0.01$; ***, $P < 0.001$; ns, not significant ($P > 0.05$).

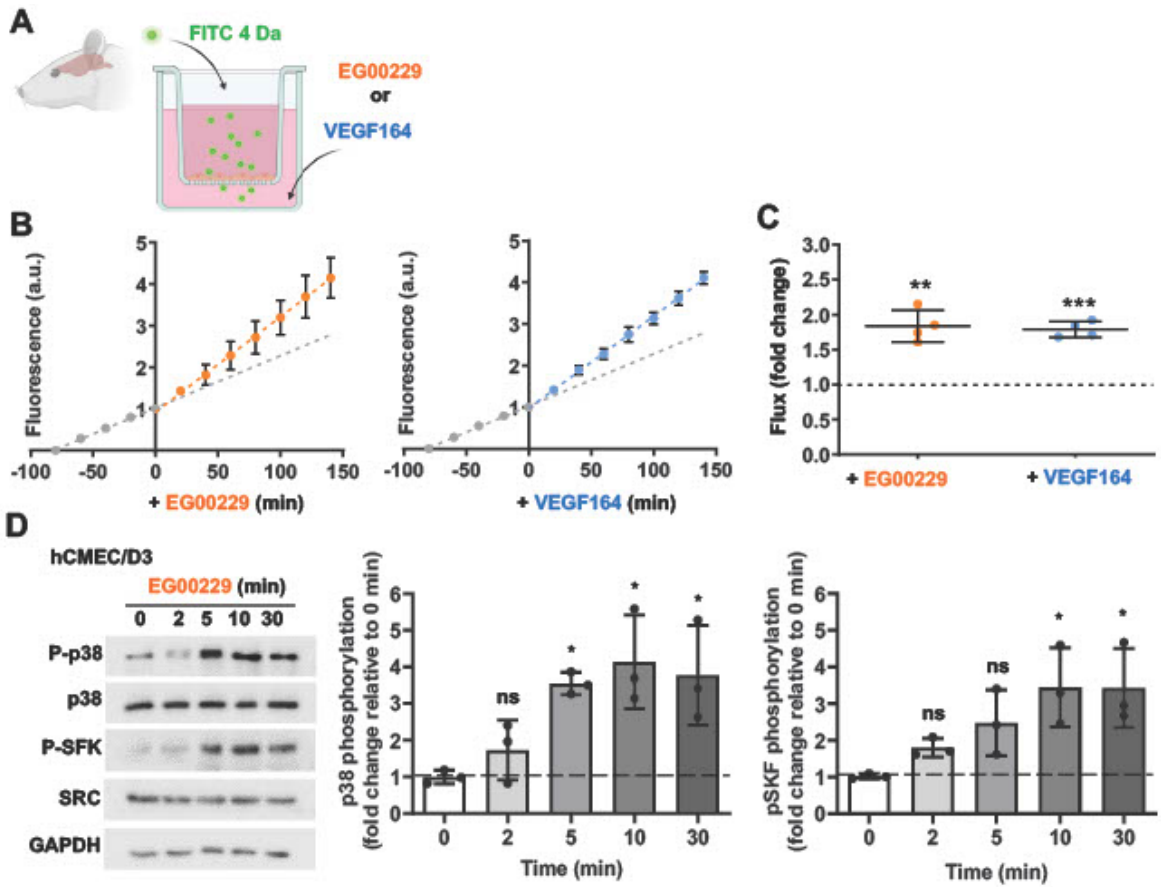

Figure S2. *EG00229 increases brain microvascular EC permeability and activates p38 and SKF.*
(**A**) Schematic of the transendothelial flux assay with brain microvascular ECs. Primary rat brain microvascular ECs were grown on permeable transwell inserts until they reached a TEER greater than 200 Ω/cm2. 4 kDa FITC dextran was then added to the apical chamber. Baseline FITC flux was recorded as the time-dependent accumulation of fluorescence in the basal chamber before adding EG00229 or VEGF164 and continued recording.
(**B,C**) EG00229 increases the permeability of brain microvascular EC monolayers. Linear regression analysis of flux over time before and after adding VEGF164 or EG00229, defined as time 0. (**B**) Data are shown as mean ± SD flux change from 4 independent experiments over time. (**C**) Data are also shown as mean fold change of flux following EG00229 or VEGF164 treatment in comparison to the baseline. Asterisks indicate statistical significance (Student's t-test): **, $P < 0.01$; ***, $P < 0.001$; ns, not significant ($P > 0.05$).
(**D**) EG00229 activates p38 and SFK in human ECs. Confluent hCMEC/D3 were treated with EG00229 for the indicated times. Cell lysates were used for immunoblotting with the indicated antibodies, followed by quantification of pixel intensities for P-P38 and P-SFK relative to total P38 and SRC pixel intensities, respectively. GAPDH was used as a loading control. Data are shown as mean fold change ± SD. P38 and SFK phosphorylation levels after EG0229 treatment were quantified at different time points relative to 0 min. Asterisks indicate significant P-values for phosphorylation induction after EG00229 treatment (one-way ANOVA): *, $P < 0.05$; **, $P < 0.01$; ns, not significant ($P > 0.05$).

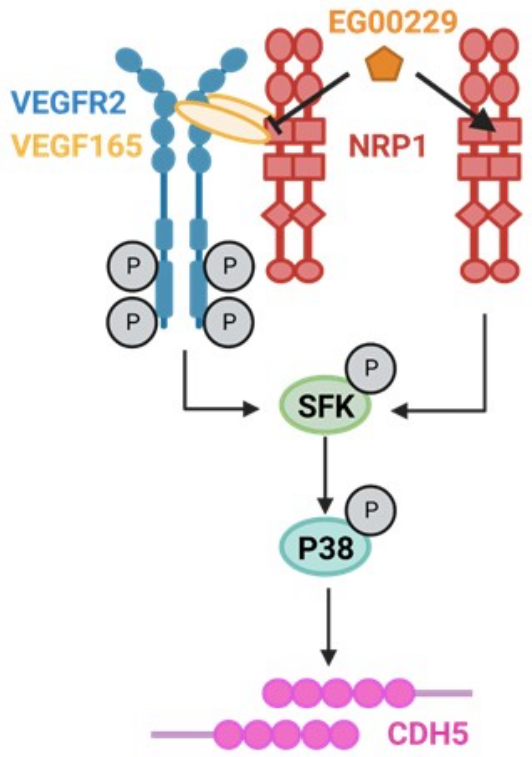

Figure S3. *Working model for VEGF164- vs. EG00229-induced signalling in brain and retina ECs.* VEGF164 binds to VEGFR2 and NRP1 to induce complex formation, whereas EG00229 binds to NRP1 alone and impairs its interaction with VEGF164. VEGF164 or EG00229 binding to their receptors activates SFK and downstream p38 signalling, which in turn induces CDH5 rearrangements and opening of adherens junctions. Created with BioRender.